nature communications

Article

https://doi.org/10.1038/s41467-026-69164-y

Anthropogenic climate change drives rising global heat stress and its spatial inequality

Received: 11 January 2025

Accepted: 26 January 2026

Published online: 03 February 2026

Check for updates

Jian Peng[1] ✉, Qi Wang[2,3], Zhiwei Yang[1], Jianquan Dong[4], Xiaoyu Yu[1] & Jonathan Corcoran[5]

Global heat stress is intensifying under climate change, yet the relative roles of natural and anthropogenic forcing remain insufficiently quantified. Here, we show that global heat stress trend, assessed with the Universal Thermal Climate Index, increases markedly over the past four decades, with 52% of land area experiencing rises in mean heat stress intensity and 67% showing increases in extreme heat stress days. We find that anthropogenic climate change overwhelmingly dominates these trends, with the land area it dominates nearly twice as large as that dominated by natural climate change. Anthropogenic climate change also results in pronounced spatial inequality in heat stress trends across different economies, with low-income economies experiencing a growth rate two to three times higher than that of high-income economies. These findings demonstrate that human-induced climate change is amplifying global heat stress while deepening existing spatial inequalities, underscoring the urgency of equitable climate change adaptation.

Global heat stress is escalating, with extreme high temperatures and prolonged heat waves becoming increasingly frequent, intense, and persistent, resulting in severe consequences for human health and socioeconomic stability[1,2]. This increase in heat stress is largely driven by climate change, which is intensifying climatic extremes across a growing number of regions, particularly within tropical and subtropical climates[3]. In these regions, the combined effects of high temperatures and high humidity are pushing ambient heat levels dangerously close to human survival thresholds[4]. Additionally, evidence highlights the growing unevenness in how climate change impacts heat stress, disproportionately burdening low- and middle-income economies, exacerbating international disparities, and intensifying global environmental injustice[5]. As global temperatures rise, inequalities in heat stress exposure are projected to widen, necessitating immediate and informed interventions to ensure equitable climate change adaptation. Comprehensive assessments of heat stress under climate change provide the theoretical and practical foundations necessary for effective mitigation, which are also essential for informing policies aimed at safeguarding vulnerable populations and promoting environmental justice.

Recent studies have increasingly emphasized the importance of moving beyond conventional temperature-based analyses to evaluate human thermal comfort more comprehensively[6,7]. Metrics such as the Universal Thermal Climate Index (UTCI), wet-bulb temperature, and net effective temperature have emerged as critical tools for capturing complex interactions between temperature, humidity, radiation, and wind, providing a more accurate assessment of thermal comfort and human health[8,9]. Despite these advancements, critical research gaps remain. In particular, existing studies have predominantly investigated heat stress using simple temperature-based indices[10,11], with limited exploration of historical variability and spatial inequality using human-perceived thermal stress indicators. Furthermore, although there is a broad consensus on climate change's general role in intensifying heat stress, the precise contributions and relative importance of anthropogenic versus natural climate change remain inadequately quantified, particularly in terms of their differential impacts across socioeconomically diverse regions[2].

Recent literature has underscored that heat stress impacts are intricately linked with socioeconomic vulnerabilities[5], and has stressed

[1]Laboratory for Earth Surface Processes, Ministry of Education, College of Urban and Environmental Sciences, Peking University, Beijing, China. [2]Key Laboratory for Environmental and Urban Sciences, School of Urban Planning and Design, Shenzhen Graduate School, Peking University, Shenzhen, China. [3]Homedale Urban Planning & Architects CO. LTD. of BMICPD, Beijing, China. [4]School of Landscape Architecture, Beijing Forestry University, Beijing, China. [5]School of the Environment, The University of Queensland, Brisbane, QLD, Australia. ✉e-mail: jianpeng@urban.pku.edu.cn

the need to evaluate spatial inequality in heat stress trend across economies by considering both anthropogenic and natural climate change[12]. Studies have indicated pronounced disparities in adaptive capacities and vulnerability to heat stress, particularly in South Asia, Africa, and South America, where extreme heat events have increasingly threatened economic stability and public health[13]. Thus, a comprehensive global assessment of heat stress trends, their climatic drivers, and associated spatial inequality across economies is essential for formulating targeted mitigation strategies and effective adaptation policies.

Addressing these research gaps requires an examination in three key issues: (1) detailed characterization of the spatial and temporal dynamics of global heat stress using indicators reflective of human thermal comfort; (2) rigorous attribution of heat stress trend to anthropogenic and natural climatic change; and (3) an explicit analysis of spatial inequality in heat stress trend across economies differing in socioeconomic development. Addressing these issues will advance the understanding of global heat stress patterns, inform policy-making targeted at reducing spatial inequality, and strengthen adaptive capacity where it is most urgently needed.

In this study, we employ the UTCI to quantify global heat stress trends from 1981 to 2020. Using statistical and machine-learning approaches, including the Theil-Sen estimator, Mann–Kendall trend analysis, and the Light Gradient Boosting Machine (LightGBM), we attribute heat stress trend to anthropogenic and natural climate drivers. We further assess how these contributions vary across economies classified by the World Bank as high-income (H), upper-middle-income (UM), lower-middle-income (LM), and low-income (L) groups[14]. Together, this framework identifies the distinct roles of anthropogenic and natural climate change in shaping global heat stress intensification and quantifies the extent to which these drivers differentially affect economies at varying levels of socioeconomic development, thereby informing assessments of climate-related environmental justice.

Results

Global mean heat stress intensity and extreme heat stress days

We quantified the mean heat stress intensity and extreme heat stress days using UTCI data, applying the Theil–Sen estimator combined with the Mann–Kendall trend test to calculate global heat stress trend from 1981 to 2020 (Table 1). We also compared the differences in trends for each two-decade period to identify land area and regions where heat stress increased (Figs. 1 and 2). Regions were defined using the IPCC AR6 reference land regions (Supplementary Fig. 1). The results showed that the border areas of Eurasia and North Africa exhibited a higher increasing trend in mean heat stress intensity (Fig. 1a). Approximately 52% of global land area showed a significant increase in mean heat stress intensity (Fig. 1b), with an overall trend of 0.012 °C· yr^{-1} (Fig. 1c). Notably, the annual trend in mean heat stress intensity increased over time, with a trend of 0.017 °C· yr^{-1} from 2001 to 2020, more than twice the trend from the preceding period of 1981–2000 (Table 1). A comparative analysis of regional trends over time (Fig. 1d and Supplementary Table 1) revealed that 37 regions experienced a higher pace of increase during 2001–2020 compared to 1981–2000. Eastern Australia and northern Australia, in particular, experienced the most dramatic increases in mean heat stress intensity, with trend increases for 2001–2020 of 0.082 °C· yr^{-1} and 0.071 °C· yr^{-1} relative to 1981–2000, respectively. Comparable surges were evident in western Southern Africa (trend rising from 0 to 0.031 °C· yr^{-1}) and eastern Southern Africa (from −0.006 to 0.021 °C· yr^{-1}). In north-eastern South America, the trend accelerated from 0.011 to 0.030 °C· yr^{-1}, and in north-western South America, it increased from 0.001 to 0.021 °C· yr^{-1}, underscoring that Africa and South America were experiencing increases on par with those in Australia.

The increasing trend of extreme heat stress days was notably higher in the land area between the 30° north and south latitudes (Fig. 2a). Approximately 67% of global land area showed a significant increasing trend in extreme heat stress days (Fig. 2b), with a trend of about 0.429 days· yr^{-1} (Fig. 2c). Moreover, the annual trend in extreme heat stress days increased over time, with a trend of 0.772 days· yr^{-1} from 2001 to 2020, nearly three times the trend observed between 1981 and 2000 (Table 1). A comparison of regional trends over time (Fig. 2d and Supplementary Table 2) revealed that 40 regions experienced a higher pace of increase in the latter period. Northern Australia experienced the largest increase, with the trend increase of 2.248 days· yr^{-1} for 2001–2020 relative to 1981–2000. The low-latitude tropics recorded similarly steep rises. For example, Central Africa reached +2.029 days· yr^{-1}, with North-Eastern Africa +1.494 days· yr^{-1}, and Madagascar +1.444 days· yr^{-1}. Similarly, pronounced surges were observed across tropical South America. The North South America sub-region showed an increment of +1.584 days· yr^{-1}, and the South American Monsoon zone rose by +1.334 days· yr^{-1}, with the North-Eastern South America by +1.323 days· yr^{-1}. These values confirmed that the rapid escalation in extreme heat stress days was also occurring across equatorial Africa as well as tropical South America. Additionally, the increasing trend in extreme heat stress days globally was more pronounced than that of the trend in mean heat stress intensity, suggesting that future climate change may lead to disproportionately severe impacts from extreme heat.

Impacts of natural and anthropogenic climate change on global heat stress trend

We employed LightGBM to investigate the relationship between climate change and heat stress trend. Then, using counterfactual analysis, we constructed three scenarios of historical scenario (ALL), natural-only scenario (NAT), and anthropogenic-only scenario (Anthro), to quantify the relative contributions of natural and anthropogenic climate change to heat stress trend, thereby distinguishing their effects.

Increasing temperatures were the primary factor affecting heat stress trend, with temperature trends explaining 28% and 35% of the variation in global mean heat stress intensity and extreme heat stress days, respectively. Furthermore, the impact of anthropogenic climate change on heat stress trend was found to be much greater than that of natural climate change (Fig. 3). For the period 1981–2000, the trends attributable to anthropogenic climate change were 0.012 °C· yr^{-1} for mean intensity and 0.267 days· yr^{-1} for extreme heat stress days. These values exceeded the trends due to natural climate change by 0.017 °C· yr^{-1} and 0.302 days· yr^{-1}, respectively. From 2001 to 2020, the anthropogenic trends increased to 0.015 °C· yr^{-1} and 0.491 days· yr^{-1}, exceeding the natural trends by 0.014 °C· yr^{-1} and 0.316 days· yr^{-1}. Regions such as Northeastern South America, Central Africa, and Northern Australia experienced both higher mean heat stress intensity and extreme heat stress days under anthropogenic climate change (Fig. 3).

Moreover, the increases in global heat stress were predominantly driven by anthropogenic climate change, while regions with decreasing heat stress trends were largely influenced by natural climate change (Fig. 4). Notably, the geographical area experiencing increases driven by anthropogenic climate change was approximately twice as large as the area affected by natural climate change and was predominantly located between 30° north and south latitude. Within this latitudinal band, regions such as Brazil and many parts of equatorial Africa showed a particularly strong anthropogenic signal. Conversely, areas dominated by natural climate change-related decreases in heat stress were about two to seven times larger than those affected by anthropogenic climate change, which were mostly situated at high latitudes, such as northern North America and the Russian Arctic.

Spatial inequality in global heat stress trend across economies

To investigate the spatial inequality in global heat stress trend, we analyzed the differences in heat stress trend among economies with

Table 1 | Trends in mean heat stress intensity and extreme heat stress days

Global heat stress	1981–2020	1981–2000	2001–2020
Mean heat stress intensity (°C· yr^{-1})	0.012***	0.008***	0.017***
Extreme heat stress days (days· yr^{-1})	0.429***	0.260***	0.772***

***p < 0.001

varying levels of socioeconomic development (Fig. 5a), under three scenarios (ALL, NAT, and Anthro). This was conducted at the economy level using the concentration index to quantify spatial inequality.

Heat stress trend showed divergent patterns across economies, dependent on their level of socioeconomic development. Under Anthro scenario, low-income and lower-middle-income economies experienced higher trends in the increase of heat stress compared to high-income and upper-middle-income economies. Specifically, low-income economies showed increases approximately two to three times greater than those in high-income economies (Fig. 5b–e). Furthermore, the concentration index for heat stress trend under the Anthro scenario was positive, whereas that under NAT scenario was negative (Fig. 5f, g). These results indicated that anthropogenic climate change was the primary driver of spatial inequality in heat stress trend across economies. In contrast, natural climate change tended to partially offset this spatial inequality.

Moreover, under Anthro scenario, spatial inequality in heat stress trend across economies had intensified between 2001 and 2020, and spatial inequality across economies in extreme heat stress days was higher than that in mean heat stress intensity, with the concentration index for extreme heat stress days being about two to four times that of mean heat stress intensity. Under ALL scenario, which combined both natural and anthropogenic climate change, mean heat stress intensity trend did not show significant spatial inequality at the global economy level. By contrast, extreme heat stress days trend revealed substantial spatial inequality across economies. This contrast indicates that extreme heat stress days have more adverse impacts on low-income economies than changes in mean heat stress intensity.

Discussion

Amidst global warming, human thermal stress is intensifying, impacting economies worldwide in increasingly uneven ways[12]. A comprehensive global assessment of heat stress trends under climate change is crucial for providing both theoretical and practical support to mitigate heat stress. Moving beyond studies that focused on air temperature extremes, this study emphasized human thermal comfort, more directly linked to human health. We quantified global heat stress using human comfort indicators, i.e., mean heat stress intensity and extreme heat stress days. A pervasive rise in heat stress has occurred across every inhabited continent over the past four decades, as evidenced by increases in the annual hours above UTCI 32 °C in regions ranging from Europe (1979–2019)[15], to the Caribbean and subtropical Atlantic[16], South America[17], and even high-latitude Beringia[18]. Our findings that 52% and 67% of global land area showed a significant increase in mean heat stress intensity and extreme heat stress days, respectively, are consistent with a broad empirical consensus. This trend is projected to intensify, which was reported that even under 2 °C warming scenarios, exposure to dangerous heat stress levels might increase dramatically in the tropics and midlatitudes, with a tenfold increase likely in many areas by 2100[19].

We quantified the differential impacts of natural and anthropogenic climate change on heat stress trend and spatial inequality in heat stress trend across economies. A key finding is that anthropogenic climate change exerted a greater influence than natural climate change on both mean and extreme heat stress, underscoring its dominant role in reshaping global heat stress patterns. Additionally, the effect of anthropogenic climate change on extreme heat stress days was particularly pronounced. This phenomenon indicates that anthropogenic climate change is elevating the frequency and intensity of extreme weather events, which implicates far-reaching impacts on human health, ecosystems, and socioeconomic systems. Studies have shown that specific populations, including migrants, pregnant women, and outdoor laborers, are more vulnerable to heat stress due to combined physiological and occupational exposure[20,21]. In India's coastal cities, for example, a rising Steadman Heat Stress Index indicates a substantial decline in work performance in future decades, especially under higher Shared Socioeconomic Pathways (SSP) scenarios[22]. At the global level, more than 70% of the workforce is currently exposed to severe heat risk, underscoring the critical need for global labor protection strategies under rising temperatures[23].

We found clear inequalities in the impact of climate change on global heat stress trend, particularly affecting low- and lower-middle-income economies, which experienced substantially higher increases in heat stress compared to high- and upper-middle-income economies. This disparity, primarily driven by anthropogenic climate change, poses a severe threat to the socioeconomic development and livelihoods of people in these developing countries. Many low-income and lower-middle-income economies exhibited a higher anthropogenic contribution to heat stress (e.g., Brazil and sub-Saharan African countries). This higher anthropogenic contribution is likely to translate into more severe impacts in low-income economies, because, unlike in high-income economies where adaptation measures such as widespread cooling access and health infrastructure can mitigate the impacts, low-income economies lack such protections. The urban areas in low-income economies often expand rapidly without climate-resilient planning, and labor forces are concentrated in climate-sensitive outdoor sectors, allowing the anthropogenic signal to manifest more directly and intensely[24,25]. This observation is consistent with recent regional studies demonstrating inequality in heat-related mortality and productivity. For example, in South Africa, inequality increases sharply at higher temperatures, especially affecting agricultural workers and poorer households with lower adaptive capacity[26]. In African equatorial regions, cooling demand is projected to become infeasible with traditional infrastructure, placing significant stress on energy and health systems[27]. In Brazil, studies show that heat-related excess mortality is disproportionately concentrated among older adults, historically marginalized racial groups, and low-education populations[28]. Similarly, across Latin American cities, poverty and segregation are key factors exacerbating heat-related mortality risks[29]. In Europe, regional economic damages from extreme heat have already exceeded 1% of GDP in vulnerable areas and are projected to rise without additional mitigation and adaptation[30]. Therefore, enhancing climate adaptation in low-income economies is a crucial direction for global climate policy. Specific measures to achieve this target may include increasing international financial support and promoting localized adaptation strategies. These policy recommendations aim to improve the heat stress adaptation capacity of low-income economies, thereby reducing the adverse impacts of global heat stress.

There are also several limitations to this study that require noting. Firstly, there is a need for deeper exploration of the mechanisms by which anthropogenic climate change affects heat stress trend. Specifically, heat stress trend in urban areas are driven by a combination of large-scale factors and localized urbanization effects[31,32]. Moreover, urban residents are more severely threatened by extreme heat stress due to the intensification of the urban heat island effect and the continuous expansion of urban area[33,34]. Future research is recommended to differentiate between urban and rural areas, focus on the contribution of urbanization to the increase in heat stress, and explore the impacts of various anthropogenic activities, such as urbanization

https://doi.org/10.1038/s41467-026-69164-y

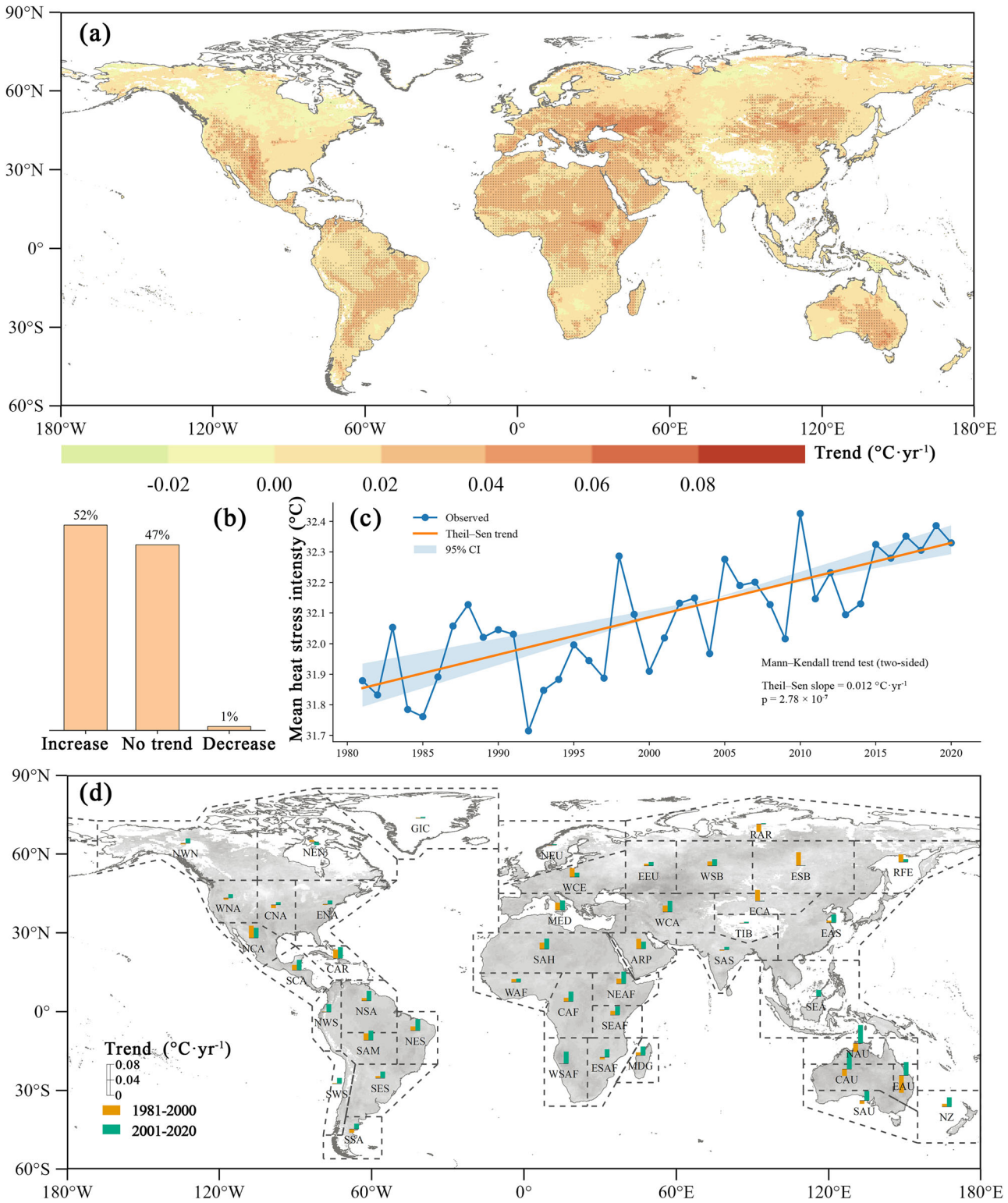

Fig. 1 | Trends in global mean heat stress intensity during 1981–2020: **a** spatial patterns (black crosses indicate significant at 0.05 level); **b** proportions for significant increase and decrease trends; **c** global annual trend; and **d** trends in different regions and periods.

processes and anthropogenic heat emissions, on heat stress trend. Secondly, while the 0.25° resolution of ERA5-HEAT provides robust global coverage, it cannot resolve microscale phenomena such as urban heat islands, fine-scale land cover heterogeneity, or localized shade effects. As a result, our findings primarily reflect broad regional trends, and caution is warranted when interpreting results for individual cities or suburban locales in low- and middle-income economies. We recommend future work to employ high-resolution downscaled UTCI products or station networks to capture intra-urban variability.

Thirdly, our analysis focused solely on spatial inequality in heat stress trend across economies, but different populations within the same geographical area may have varied adaptations to heat stress due to physiological and socioeconomic differences, resulting in differing vulnerabilities when facing the same heat stress[35]. Future research may

https://doi.org/10.1038/s41467-026-69164-y

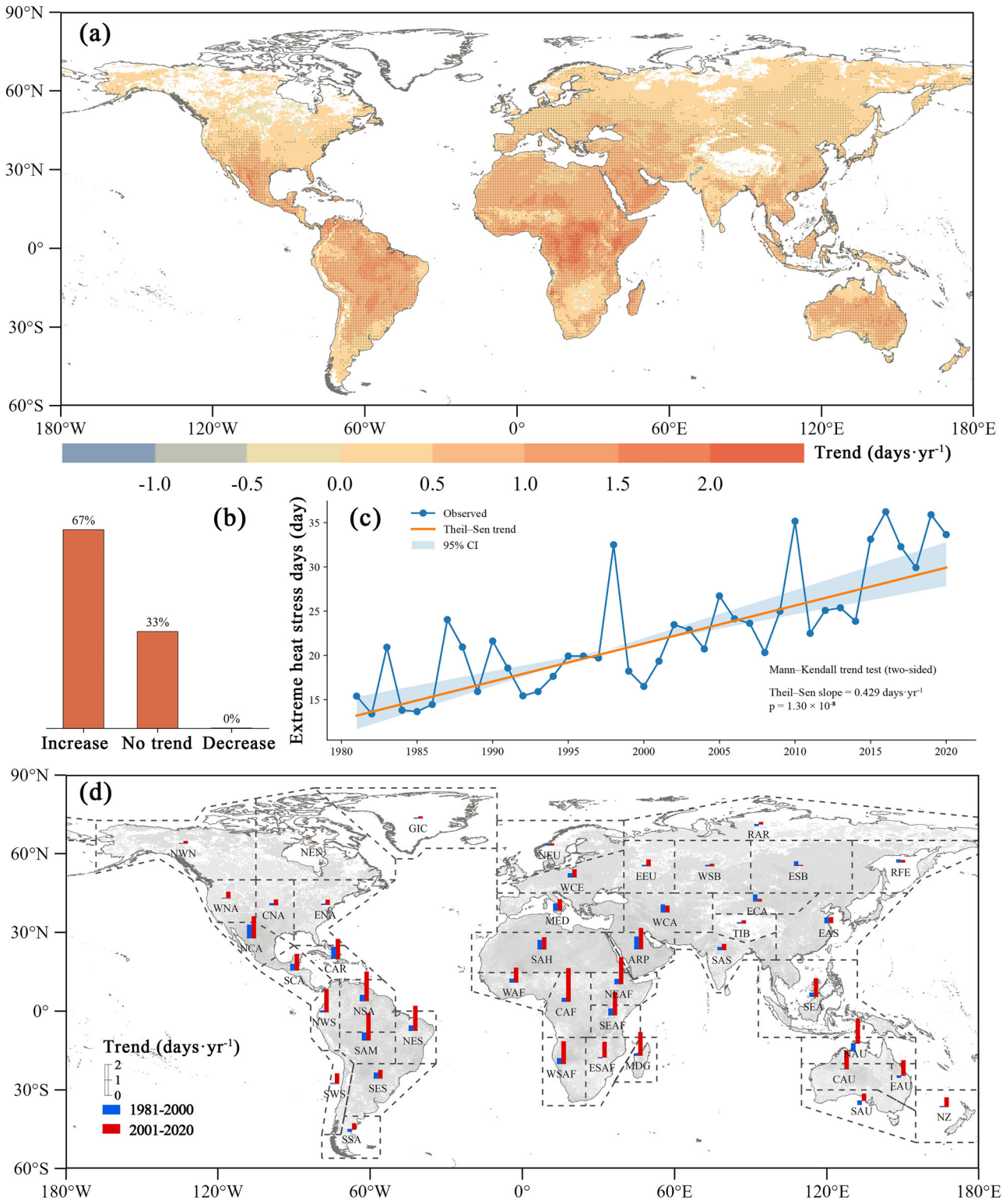

Fig. 2 | Trends in global extreme heat stress days during 1981–2020: **a** spatial patterns (black crosses indicate significant at 0.05 level); **b** proportions for significant increase and decrease trends; **c** global annual trend; and **d** trends in different regions and periods.

consider differentiating among various vulnerable groups within economies or subnational areas, such as different ethnicities, age groups, occupational groups, and educational groups[2,36]. This would allow for a more nuanced assessment of spatial inequality in heat stress trend by considering the specific vulnerabilities and adaptation capacities of different population groups. Lastly, in line with recent IPCC AR6 findings[37], it is increasingly evident that heat stress does not operate in isolation. Regions facing rapid warming also experience compound and cascading climate risks, such as the co-occurrence of heatwaves with drought, wildfire, or extreme rainfall. These intersecting hazards, often reinforced by weak governance or infrastructure, intensify vulnerability across multiple sectors. For instance, South Asia and West Africa have reported simultaneous exposure to heat extremes and rainfall anomalies that overwhelmed coping systems[38,39]. Understanding spatial inequality in

https://doi.org/10.1038/s41467-026-69164-y

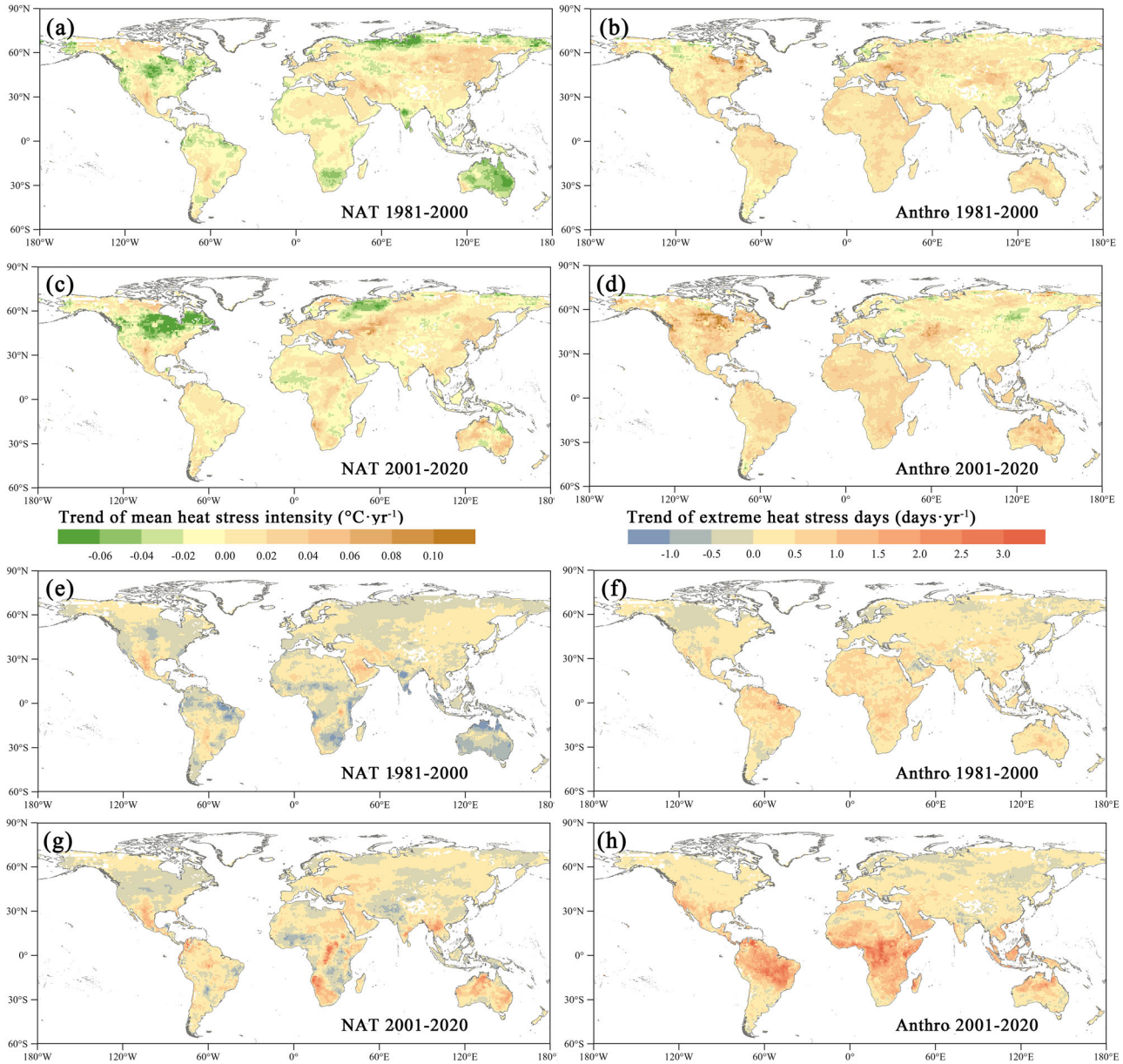

Fig. 3 | Trends in mean heat stress intensity and extreme heat stress days under natural-only scenario (NAT), and anthropogenic-only scenario (Anthro): **a**, **b** trend of mean heat stress intensity under NAT and Anthro scenarios during 1981–2000; **c**, **d** trend of mean heat stress intensity under NAT and Anthro scenarios during 2001–2020; **e**, **f** trend of extreme heat stress days under NAT and Anthro scenarios during 1981–2000; and **g**, **h** trend of extreme heat stress days under NAT and Anthro scenarios during 2001–2020.

heat stress trend must therefore be placed within a broader multi-hazard perspective that reflects the full spectrum of climate-related threats.

Methods

To quantify and attribute global heat stress trend, we implemented a five-step workflow. Firstly, we extracted daily maximum UTCI values from the ERA5-HEAT reanalysis (1981–2020) to compute yearly mean heat stress intensity and extreme heat stress days. Secondly, we quantified temporal trends using the robust Theil-Sen slope estimator paired with the Mann–Kendall non-parametric test to assess statistical significance. Thirdly, we trained a LightGBM model, chosen for its speed, scalability, and high accuracy in nonlinear regression, to link local trends in temperature and humidity, as well as geographical coordinates to observed heat stress trend. Fourthly, we disentangled anthropogenic from natural climate change by constructing NAT and Anthro scenarios using counterfactual analysis. Finally, we assessed spatial inequality in heat stress trend across economies by ranking economies according to 2020 GDP per capita and computing concentration index under ALL, NAT, and Anthro scenarios.

Data preprocessing

The UTCI has been widely used to quantify changes in heat stress and human heat exposure[6,40]. UTCI is a thermophysiological index designed to reflect human thermal comfort by incorporating air temperature, humidity, wind, and radiation into a biophysical heat-exchange model calibrated on human physiology[41,42]. ERA5-HEAT is the first set of global historical UTCI raster data, which is based on ERA5 meteorological reanalysis data[43], and offers a temporal resolution of hour-by-hour and a spatial resolution of 0.25°[44]. We selected 40 years of ERA5-HEAT data, spanning 1981 to 2020. From this dataset, we extracted daily maximum UTCI values from the hour-by-hour data to characterize heat stress.

https://doi.org/10.1038/s41467-026-69164-y

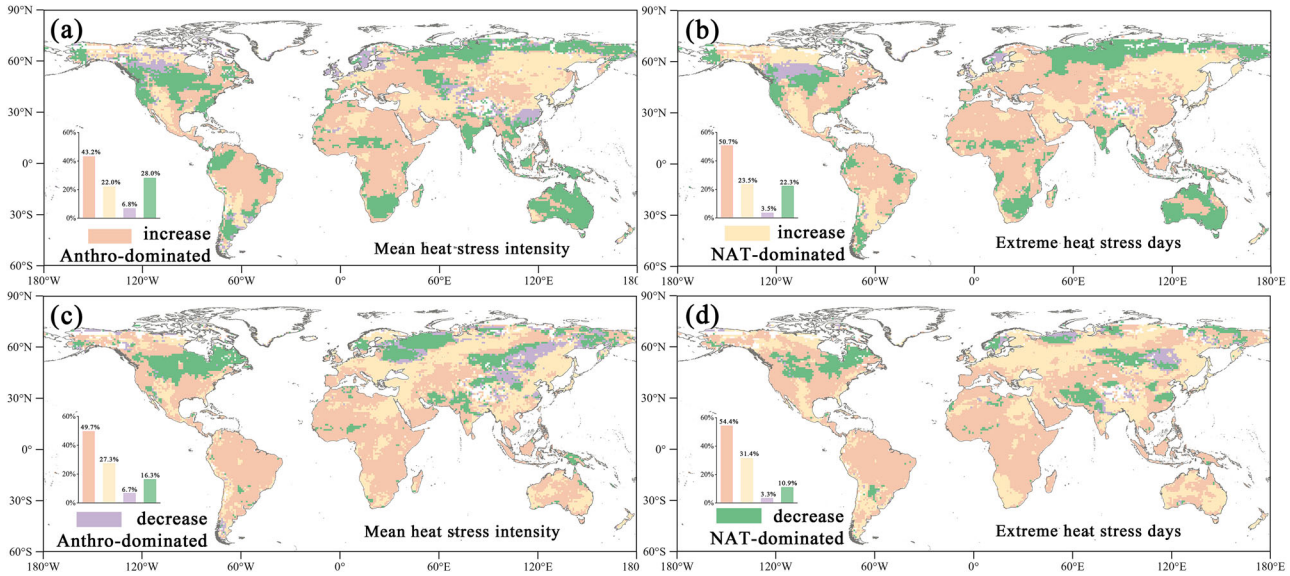

Fig. 4 | Distribution and area proportions of the change types in global mean heat stress intensity and extreme heat stress days: **a**, **b** change types for mean heat stress intensity and extreme heat stress days during 1981–2000; and **c**, **d** change types for mean heat stress intensity and extreme heat stress days during 2001–2020. Change types are classified into four categories based on the dominant driver-anthropogenic climate change (Anthro-dominated) versus natural climate change (NAT-dominated) and the trend direction (increase/decrease). Bar charts indicate the areal proportion of each change type.

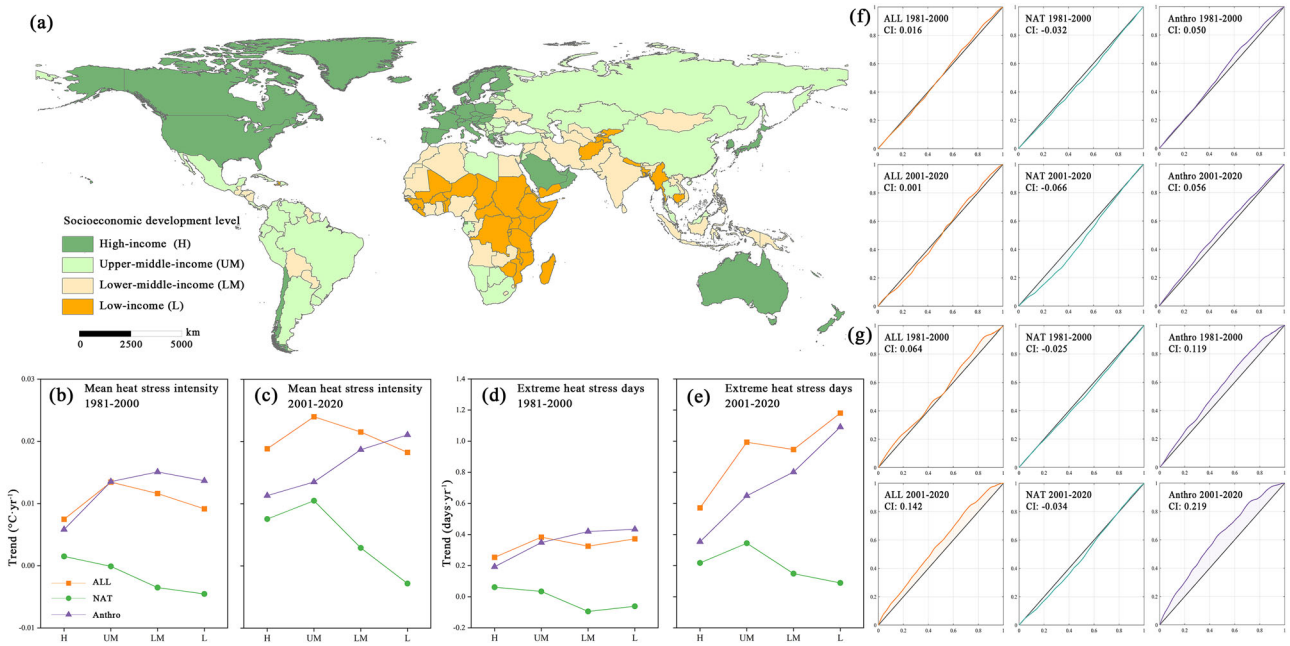

Fig. 5 | Trends and concentration curves of global mean heat stress intensity and extreme heat stress days under historical scenario (ALL), natural-only scenario (NAT), and anthropogenic-only scenario (Anthro) for four socioeconomic development levels: **a** global grouping of economies at four socioeconomic development levels; **b**, **c** trends of mean heat stress intensity under three scenarios for the four categories of economies for 1981–2000 and 2001–2020, respectively; **d**, **e** trends of extreme heat stress days under three scenarios for the four categories of economies for 1981–2000 and 2001–2020, respectively; **f** concentration curves of trends in mean heat stress intensity for the three scenarios during 1981–2000 and 2001–2020, respectively; and **g** concentration curves of trends in extreme heat stress days for the three scenarios during 1981–2000 and 2001–2020, respectively.

Meteorological data were obtained from the ERA5-Land and ERA5 reanalysis datasets produced by the European Centre for Medium-Range Weather Forecasts. We selected temperature and relative humidity data from the period 1981–2020, both with an hour-by-hour temporal resolution. Temperature data were sourced from the ERA5-Land dataset, which has a spatial resolution of 0.1°. From this dataset, daily mean temperature values were extracted to calculate annual mean temperatures, which were then resampled to a 0.25° spatial resolution. Relative humidity data were obtained from the ERA5 reanalysis dataset, which has a spatial resolution of 0.25°. Daily mean relative humidity values were extracted to calculate annual mean humidity.

Model data were sourced from the Coupled Model Intercomparison Project Phase 6 (CMIP6). The Detection and Attribution Model Intercomparison Project (DAMIP), a component of CMIP6, was utilized to assess the contributions of various factors to global climate change. DAMIP provides four sets of experiments: historical simulation, natural-forcing historical simulation, greenhouse-gas-forcing historical simulation, and aerosol-forcing historical simulation. The historical simulation data spans from 1961 to 2014, while the natural-forcing historical simulation, greenhouse-gas-forcing historical simulation, and aerosol-forcing historical simulation data cover the years from 1961 to 2020. We selected the historical simulation and natural-forcing historical simulation data from nine different climate models within DAMIP (Supplementary Table 3). Additionally, future climate projections based on the SSP and Representative Concentration Pathways (RCP) are provided by the CMIP6 Scenario Model Intercomparison Projection (ScenarioMIP). We chose the SSP2-4.5 (Medium Development with Medium Radiative Forcing), which is considered a continuation of the historical scenario[45], for the period of 2015–2020 to complement the historical climate data.

Definition of heat stress

We identified heat stress days and extreme heat stress days using daily maximum UTCI values. Researches have consistently demonstrated that when the UTCI exceeds 26 °C, the human body experiences significant physiological responses, such as an increased sweating rate and elevated core body temperature, which can lead to discomfort, illness, and even death[46]. Consequently, we defined heat stress days as those with a daily maximum UTCI greater than 26 °C. We emphasized that although this threshold may frequently be exceeded in tropical zones, our focus lies on analyzing temporal changes in heat stress intensity and frequency over time rather than absolute values. Additionally, extreme heat stress can have more severe effects on human health[47], and thus, we further identified extreme heat stress days using a relative threshold approach. While the official UTCI classification designates >46 °C as 'Extreme Heat Stress', this absolute threshold does not account for local acclimatization or climate variability. Therefore, we employed a grid-specific and time-adaptive relative threshold, defined as the 90th percentile of daily maximum UTCI values calculated within a 15-day moving window[48].

We assessed heat stress by examining both mean heat stress intensity and extreme heat stress days. (1) Mean heat stress intensity: This is characterized by the average daily maximum UTCI of heat stress days. Higher mean daily UTCI values indicate greater heat stress, suggesting that human societies are exposed to higher heat stress. (2) Extreme heat stress days: This is characterized by the number of days experiencing extreme heat stress. Since extreme heat stress can have more severe impacts on human health and society[47], an increase in the number of extreme heat stress days implies a higher risk of mortality[49]. The number of days was chosen to represent extreme heat stress because the mean UTCI values for extreme heat stress days tend to show less variability and are not as indicative of the overall impact as the extreme heat stress days[33]. We employed Theil-Sen estimator, a robust non-parametric method for estimating linear trends, combined with the Mann–Kendall test, a non-parametric significance test for trend detection, to quantitatively analyze the temporal trends in both mean heat stress intensity and extreme heat stress days from 1981 to 2020[50].

Linking climate change to heat stress trend

To relate climate change to heat stress trend, we employed a LightGBM model. We selected LightGBM, a histogram-based Gradient Boosting Decision Tree (GBDT) implementation, because it delivers state-of-the-art accuracy, exceptional training speed (up to 20× faster than traditional GBDT)[51], and efficient handling of large datasets with high feature dimensions[52]. The model is built upon a gradient boosting framework as Eq. (1).

$$F_m(x) = F_{m-1}(x) + \nu \sum_{k=1}^{K} \gamma_{mk} I\left(x \in R_{mk}\right) \tag{1}$$

where $F_m(x)$ is the ensemble prediction after adding the m-th tree. $F_{m-1}(x)$ is the prediction from the previous boosting iteration. ν is the learning rate. K is the number of terminal leaves in the m-th tree, γ_{mk} is leaf weight, and R_{mk} is the corresponding input region (leaf partition) in the feature space defined by the splits of the m-th tree. $I\left(x \in R_{mk}\right)$ is an indicator function that equals 1 if the sample x falls into region R_{mk}, and 0 otherwise.

We used this model to estimate the trends in mean heat stress intensity and extreme heat stress days as response variables. Predictors included: trends in temperature and humidity, their climatological means, and geographical coordinates[53]. Model validation was performed via 10-fold cross-validation. The R^2 for test sets was 0.865 (mean heat stress intensity) and 0.917 (extreme heat stress days). Feature importance results indicated that temperature trend (28%) and longitude (22%) were most important for mean heat stress intensity change, while temperature trend alone dominated changes in extreme heat stress days change (35%).

Counterfactual analysis

To construct the climate series under the counterfactual condition, we applied a delta bias correction approach[45,54]. Specifically, we calculated temperature and relative humidity under the counterfactual condition using Eqs. (2) and (3).

$$T_{\text{counterfactual}}(t) = T_{\text{ERA5}}(t) - \left[T_{\text{DAMIP\_historical}}(t) - T_{\text{DAMIP\_nat}}(t)\right] \tag{2}$$

$$RH_{\text{counterfactual}}(t) = RH_{\text{ERA5}}(t) - \left[RH_{\text{DAMIP\_historical}}(t) - RH_{\text{DAMIP\_nat}}(t)\right] \tag{3}$$

Where, $T_{\text{counterfactual}}(t)$ and $RH_{\text{counterfactual}}(t)$ are the temperature and relative humidity series under counterfactual condition at time t; $T_{\text{ERA5}}(t)$ and $RH_{\text{ERA5}}(t)$ are daily values from ERA5-Land and ERA5 reanalysis datasets; $T_{\text{DAMIP\_historical}}(t)$ and $RH_{\text{DAMIP\_historical}}(t)$ are ensemble mean DAMIP historical simulation; and $T_{\text{DAMIP\_nat}}(t)$ and $RH_{\text{DAMIP\_nat}}(t)$ are ensemble mean DAMIP natural-forcing historical simulation. The temperature and relative humidity series of counterfactual condition were not used to recalculate synthetic UTCI directly, but were used as inputs to the trained LightGBM model to predict heat stress trend under counterfactual condition.

To distinguish the contributions of natural and anthropogenic climate change to heat stress trends, we defined three scenarios as follows:

ALL scenario: heat stress trends driven by the factual climate change, incorporating both natural and anthropogenic climate change, as represented by ERA5-HEAT.

NAT scenario: heat stress trends driven by natural climate change alone, predicted under the counterfactual natural-only climate series.

Anthro scenario: heat stress trends attributable solely to anthropogenic climate change, estimated by removing the NAT scenario component from the ALL scenario component.

Spatial inequality assessment

We assessed spatial inequality in heat stress trend across economies with various levels of socioeconomic development by plotting concentration curves for economy under three scenarios (ALL, NAT, and Anthro). These concentration curves illustrate how heat stress trend is distributed across economies with various socioeconomic statuses. For low-income economies, lower levels of socioeconomic development generally correspond to a reduced capacity to cope with heat

stress, meaning these countries have lower adaptive capacity. As a result, increases in heat stress pose a greater risk to these countries, exacerbating their vulnerability to heat-related impacts. Therefore, increase in heat stress that disproportionately affects economies with lower socioeconomic development is considered indicative of growing spatial inequality in global heat stress.

Specifically, to measure spatial inequality in heat stress trend across economies, we ranked 157 economies in order of GDP per capita and plotted concentration curves based on the cumulative change in heat stress corresponding to the cumulative percentile of the number of economies, ordered from the poorest to the richest. Concentration index (CI) serves as a measure of spatial inequality in heat stress trend which is calculated using Eq. (4), through dividing the area between the concentration curve and the line of equality by the area above the line of equality[55].

$$\mathrm{CI} = 2\int_0^1 [L(p) - p]dp \tag{4}$$

Where $L(p)$ is the concentration curve and p is the cumulative proportion of economies. CI ranges from −1 to 1, with positive values indicating that the curve is above the line of equality and negative values indicating it is below. A concentration index closer to 1 signifies greater spatial inequality in heat stress trend across economies, with a special threat to low-income economics. Because the concentration curve requires non-negative variables, we applied the maximum–minimum normalization method to normalize the trends in mean heat stress intensity and extreme heat stress days to the range of [0–1]. Under this context, the diagonal line represents a uniform distribution of heat stress trend across economies, indicating absolute equality. If the concentration curve lies above the diagonal, it suggests that poorer economies have experienced more intense trends in heat stress. Conversely, if the curve is below the diagonal, it indicates that richer economies have experienced more intense trends in heat stress.

Reporting summary

Further information on research design is available in the Nature Portfolio Reporting Summary linked to this article.

Data availability

We used the data from the following sources in our analysis. The UTCI data were derived from the ERA5-HEAT dataset (https://cds.climate.copernicus.eu/cdsapp#!/dataset/derived-utci-historical). Temperature data were derived from the ERA5-Land dataset (https://cds.climate.copernicus.eu/cdsapp#!/dataset/reanalysis-era5-land). Relative humidity data were derived from the ERA5 reanalysis dataset (https://cds.climate.copernicus.eu/cdsapp#!/dataset/reanalysis-era5-pressure-levels). The SSP2-4.5 scenario data were derived from the CMIP6. Source data are provided with this paper.

Code availability

The codes generated in this study have been deposited in the following GitHub repository: https://github.com/YZW-D/anthropogenic-climate-change.

References

1. de Bont, J. et al. Impact of heatwaves on all-cause mortality in India: a comprehensive multi-city study. *Environ. Int.* **184**, 108461 (2024).
2. Lenton, T. M. et al. Quantifying the human cost of global warming. *Nat. Sustain.* **6**, 1237–1247 (2023).
3. Thompson, V. et al. The most at-risk regions in the world for high-impact heatwaves. *Nat. Commun.* **14**, 2152 (2023).
4. Vecellio, D. J., Kong, Q., Kenney, W. L. & Huber, M. Greatly enhanced risk to humans as a consequence of empirically determined lower moist heat stress tolerance. *Proc. Natl. Acad. Sci. USA* **120**, e2305427120 (2023).
5. Harrington, L. J. et al. Poorest countries experience earlier anthropogenic emergence of daily temperature extremes. *Environ. Res. Lett.* **11**, 055007 (2016).
6. Yang, Z., Peng, J., Jiang, S., Yu, X. & Hu, T. Optimizing building spatial morphology to alleviate human thermal stress. *Sustain. Cities Soc.* **106**, 105386 (2024).
7. Silva, T., Lopes, A., Vasconcelos, J. & Morgado, P. Thermal preference and pleasantness of a students' population in a coastal urban area during summer. *Discov. Cities* **1**, 19 (2024).
8. Dong, J., Brönnimann, S., Hu, T., Liu, Y. & Peng, J. GSDM-WBT: global station-based daily maximum wet-bulb temperature data for 1981–2020. *Earth Syst. Sci. Data* **14**, 5651–5664 (2022).
9. Yang, Z. et al. Human-centered urban heat island intensity in global megacities: nonlinear response patterns and region-specific thresholds. *Environ. Sci. Technol.* **59**, 19781–19791 (2025).
10. Gasparrini, A. et al. Mortality risk attributable to high and low ambient temperature: a multicountry observational study. *Lancet* **386**, 369–375 (2015).
11. Tuholske, C. et al. Global urban population exposure to extreme heat. *Proc. Natl. Acad. Sci. USA* **118**, e2024792118 (2021).
12. Wang, Y., Zhao, N., Wu, C., Quan, J. & Chen, M. Future population exposure to heatwaves in 83 global megacities. *Sci. Total Environ.* **888**, 164142 (2023).
13. Perkins-Kirkpatrick, S. E. & Lewis, S. C. Increasing trends in regional heatwaves. *Nat. Commun.* **11**, 3357 (2020).
14. World Development Indicators | DataBank. https://databank.worldbank.org/source/world-development-indicators.
15. Antonescu, B. et al. A 41-year bioclimatology of thermal stress in Europe. *Int. J. Climatol.* **41**, 3934–3952 (2021).
16. Di Napoli, C., Allen, T., Méndez-Lázaro, P. A. & Pappenberger, F. Heat stress in the Caribbean: climatology, drivers, and trends of human biometeorology indices. *Int. J. Climatol.* **43**, 405–425 (2023).
17. Miranda, V. F. V. V. et al. Heat stress in South America over the last four decades: a bioclimatic analysis. *Theor. Appl. Climatol.* **155**, 911–928 (2024).
18. Grigorieva, E. A., Alexeev, V. A. & Walsh, J. E. Universal thermal climate index in the Arctic in an era of climate change: Alaska and Chukotka as a case study. *Int. J. Biometeorol.* **67**, 1703–1721 (2023).
19. Vargas Zeppetello, L. R., Raftery, A. E. & Battisti, D. S. Probabilistic projections of increased heat stress driven by climate change. *Commun. Earth Environ.* **3**, 1–7 (2022).
20. Amoadu, M., Ansah, E. W., Sarfo, J. O. & Hormenu, T. Impact of climate change and heat stress on workers' health and productivity: a scoping review. *J. Clim. Change Health* **12**, 100249 (2023).
21. Habibi, P. et al. Climate change and heat stress resilient outdoor workers: findings from systematic literature review. *BMC Public Health* **24**, 1711 (2024).
22. Kumar, T. V. L., Bharath, J., Filho, W. L., Barbosa, H. & Rao, K. K. Impact of climate change induced heat stress on the people working in the coastal cities of India. *Nat. Hazards* **121**, 1803–1817 (2025).
23. More than 70% of the global workforce is at risk from severe heat – report. *World Economic Forum* https://www.weforum.org/stories/2024/08/extreme-heat-workers-climate-health/ (2024).
24. Environment, U. N. Adaptation Gap Report 2023 | UNEP - UN Environment Programme. https://www.unep.org/resources/adaptation-gap-report-2023 (2023).
25. Romanello, M. et al. The 2021 report of the Lancet Countdown on health and climate change: code red for a healthy future. *Lancet* **398**, 1619–1662 (2021).

26. Dasgupta, S., Emmerling, J. & Shayegh, S. Inequality and growth impacts of climate change—insights from South Africa. *Environ. Res. Lett.* **18**, 124005 (2023).
27. Parkes, B., Buzan, J. R. & Huber, M. Heat stress in Africa under high intensity climate change. *Int. J. Biometeorol.* **66**, 1531–1545 (2022).
28. Santos et al. Twenty-first-century demographic and social inequalities of heat-related deaths in Brazilian urban areas. *PLOS ONE* **19**, e0295766 (2024).
29. Bakhtsiyarava, M. et al. Modification of temperature-related human mortality by area-level socioeconomic and demographic characteristics in Latin American cities. *Soc. Sci. Med.* **317**, 115526 (2023).
30. García-León, D. et al. Current and projected regional economic impacts of heatwaves in Europe. *Nat. Commun.* **12**, 5807 (2021).
31. Peng, J. et al. How to quantify the cooling effect of urban parks? Linking maximum and accumulation perspectives. *Remote Sens. Environ.* **252**, 112135 (2021).
32. Wang, C. et al. Assessing urban population exposure risk to extreme heat: Patterns, trends, and implications for climate resilience in China (2000–2020). *Sustain. Cities Soc.* **103**, 105260 (2024).
33. Luo, M. & Lau, N. Increasing human-perceived heat stress risks exacerbated by urbanization in China: a comparative study based on multiple metrics. *Earths Future* **9**, e2020EF001848 (2021).
34. Yang, Z. & Peng, J. Efficiency-oriented phased urban green space planning framework to mitigate heat-stress exposure. *npj Urban Sustain.* **5**, 57 (2025).
35. Yin, Y. et al. Association between ambient temperature and influenza prevalence: a nationwide time-series analysis in 201 Chinese cities from 2013 to 2018. *Environ. Int* **189**, 108783 (2024).
36. Wang, Y. et al. Global future population exposure to heatwaves. *Environ. Int.* **178**, 108049 (2023).
37. IPCC. Climate Change 2022: Impacts, Adaptation and Vulnerability, Working Group II Contribution to AR6, Cambridge University Press, Cambridge/Cambridge, UK & New York, NY, USA. (2022). https://doi.org/10.1017/9781009325844.
38. Diffenbaugh, N. S. et al. The COVID-19 lockdowns: a window into the Earth System. *Nat. Rev. Earth Environ.* **1**, 470–481 (2020).
39. Raymond, C., Matthews, T. & Horton, R. M. The emergence of heat and humidity too severe for human tolerance. *Sci. Adv.* **6**, eaaw1838 (2020).
40. Urban, A. et al. Evaluation of the ERA5 reanalysis-based Universal Thermal Climate Index on mortality data in Europe. *Environ. Res.* **198**, 111227 (2021).
41. Spangler, K. R., Liang, S. & Wellenius, G. A. Wet-bulb globe temperature, universal thermal climate index, and other heat metrics for US Counties, 2000–2020. *Sci. Data* **9**, 326 (2022).
42. Yang, Z. et al. GloUTCI-M: a global monthly 1 km universal thermal climate index dataset from 2000 to 2022. *Earth Syst. Sci. Data* **16**, 2407–2424 (2024).
43. Di Napoli, C., Barnard, C., Prudhomme, C., Cloke, H. L. & Pappenberger, F. ERA5-HEAT: a global gridded historical dataset of human thermal comfort indices from climate reanalysis. *Geosci. Data J.* **8**, 2–10 (2021).
44. Bröde, P. et al. Deriving the operational procedure for the Universal Thermal Climate Index (UTCI). *Int. J. Biometeorol.* **56**, 481–494 (2012).
45. Vicedo-Cabrera, A. M. et al. The burden of heat-related mortality attributable to recent human-induced climate change. *Nat. Clim. Chang.* **11**, 492–500 (2021).
46. Fiala, D., Havenith, G., Bröde, P., Kampmann, B. & Jendritzky, G. UTCI-Fiala multi-node model of human heat transfer and temperature regulation. *Int. J. Biometeorol.* **56**, 429–441 (2012).
47. Zhao, Q. et al. Global, regional, and national burden of mortality associated with non-optimal ambient temperatures from 2000 to 2019: a three-stage modelling study. *Lancet Planet Health* **5**, e415–e425 (2021).
48. Al-Yaari, A., Zhao, Y., Cheruy, F. & Thiery, W. Heatwave characteristics in the recent climate and at different global warming levels: a multimodel analysis at the global scale. *Earths Future* **11**, e2022EF003301 (2023).
49. Dimitrova, A. et al. Temperature-related neonatal deaths attributable to climate change in 29 low- and middle-income countries. *Nat. Commun.* **15**, 5504 (2024).
50. Peng, J. et al. Balancing the effects of forest conservation and restoration on South China Karst Greening. *Earths Future* **11**, e2023EF003487 (2023).
51. Yuan, Y. et al. Natural-anthropogenic environment interactively causes the surface urban heat island intensity variations in global climate zones. *Environ. Int.* **170**, 107574 (2022).
52. Ke, G. et al. LightGBM: a highly efficient gradient boosting decision tree. *Adv. Neural Inform. Process. Syst.* **30**, 3146–3154 (2017).
53. Peng, J. et al. Diversified evolutionary patterns of surface urban heat island in new expansion areas of 31 Chinese cities. *npj Urban Sustain.* **4**, 1–11 (2024).
54. Zhang, Y. et al. The burden of heatwave-related preterm births and associated human capital losses in China. *Nat. Commun.* **13**, 7565 (2022).
55. Chen, B. et al. Contrasting inequality in human exposure to greenspace between cities of Global North and Global South. *Nat. Commun.* **13**, 4636 (2022).

Acknowledgements

This study was financially supported by the National Natural Science Foundation of China (grant no. 42130505 to J.P.).

Author contributions

J.P. designed the research. J.P., Q.W., and Z.Y. performed the analysis, generated figures, and drafted the paper. J.D. and X.Y. helped to generate figures and revised the draft. J.C. contributed to scientific interpretations and subsequent revisions.

Competing interests

The authors declare no competing interests.

Additional information

Supplementary information The online version contains supplementary material available at https://doi.org/10.1038/s41467-026-69164-y.

Correspondence and requests for materials should be addressed to Jian Peng.

Peer review information *Nature Communications* thanks the anonymous reviewer(s) for their contribution to the peer review of this work. A peer review file is available.